Eidgenössische Technische Hochschule Zürich
Swiss Federal Institute of Technology Zurich

The Measurement of Positronium 1S-2S Spectroscopy

Summer Thesis

Yifeng Wang

wang3128@purdue.edu

Laboratory for Positron and Positronium Physics
Department of Physics | Institute for Particle Physics and Astrophysics
ETH Zürich

Supervisors:
Dr. Paolo Crivelli

December 2, 2019

Acknowledgements

I would like to thank Dr. Crivelli for giving me the chance to work in this positronium lab during summer and coordinate relevant issues. Also, his advise in the data analysis part was very valuable and insightful. Then, I would like to thank Prof. Dissetori; he interviewed me before I came to ETH and contacted Dr. Crivelli to make this summer research possible.

For the trap and buncher part, I worked mostly with Michael. I want to thank him for his patient explanation of the theoretical background and relevant engineering problem, which is very crucial to this report. Beyond physics, his versatility in electrical, mechanical, and computer fields enriched my research experience. I want to thank Lars for providing help with MATLAB simulation. I also want to thank Zakary for advising me on writing report and providing me with reference resources.

Abstract

The thesis is meant to report my contribution to the research work conducted within the positronium group at ETH. The goal of this experiment is to measure with high precision of energy of the 1S-2S excitation of positronium, which can either correct the recent experimental results of 2 sigmas [1] away from the theory or confirm the discrepancy between experiment and theory with higher confidence, for a precision of 0.5 ppb [2]. The Second-Order Doppler Effect and Stark Effect are calculated and considered based on the experiment setup [3].

The experimental apparatus consists of a ^{22}Na source of positron, a rotating magnetic trap, a voltage gate to control the release of positron, a buncher for time compression of positron beam, an elevator to accelerate the beam, a silicon target that diffuses positronium out after bombarded by the beam, a laser apparatus to excite 1S to 2S and a multi-channel-plate (MCP) for detecting 2S as *signal*.

First, the trap, buncher, and elevator were adjusted for optimization so that the 50 ns positron beam from the gate is compressed to a desired length of 15ns and less. I wrote a simulation of positrons' energy and time distribution at each critical position between the gate and the target. This software was used as the guidance for optimization and shown in chapter 4.

Second, the data were analyzed to extract the 2S positrons annihilation signal from the background and build the line-shape of the laser spectroscopy. Moreover, it is possible to conduct the other 2S-20P measurement with the same setup with only an additional laser for creating that transition as shown in Fig. 5.1 and discussed in this paper [4] by my group members.

The beam was bunched to about 15 ns when the thesis was finished and is still being improving by adjusting the bunching waveform. The data collected back then does not clearly indicate a presence of *signal*, i.e., the laser-on datasets do not have statistically more 2S annihilation events than laser-off datasets. The reasons can be the beam length was not desirable at that time, the MCP did not have spatial resolution to distinguish the excess of 2S and other miscellaneous mis-adjustment which compromised the production and detection of the 2S.

However, the MATLAB simulation can make the future adjustment controllable and the decay time in Tab. 6.1 indicates a significant shortening in positron beam length.

Contents

Chapter 1

Introduction

The study of the purely leptonic system, which consists of a particle and its anti-particle in a bounded state, can be traced back to 1934. Mohorovicic proposed the Positronium (Ps), i.e. an electron and a positron, in theory. Then, Deutsch detected Ps experimentally in 1951 [5]. This leptonic system is advantageous in precise measurement of fine structure constant, because for any two-body system the energy level and Rydberg constant is related as

$$E_i = -\frac{R_\infty hc}{n_i^2}\frac{1+\delta_i}{1+m_1/m_2}, \tag{1.1}$$

where n_i is the principle quantum number and δ_i is the theoretical correction; the determination of different energy levels can lead to a close calculation of Rydberg constant only limited by the knowledge of small theoretical correction corresponding to each level [6]. Also, Rydberg constant contains the fine structure constant [7].

$$R_\infty = \frac{m_e e^4}{8\epsilon_0^2 h^3 c} = \frac{m_e c}{2h}\left(\frac{1}{4\pi\epsilon_0}\frac{e^2}{\hbar c}\right)^2 = \frac{m_e c}{2h}\alpha^2. \tag{1.2}$$

The infinite sign indicates it is the Rydberg constant that assumes an infinite mass of one particle, i.e. a hydrogen atom with a proton having infinite mass, thus the reduced mass is just m_e. Similarly, Rydberg constant for a positronium system is one-half of that of infinity, because the reduced mass is given by $\frac{m_{e^+}m_{e^-}}{m_{e^+}+m_{e^-}} = \frac{m_e}{2}$.

Since the uncertainty of the finite nuclear size of the proton from Quantum Chromodynamics (QCD), the best hydrogen 1S-2S transition only reached a precision of 4.2 ppb [8]. For Ps, without the "finite size" problem, we can measure the energy of any two-level of transition to get the Rydberg constant and then fine structure constant. In this experiment, we chose the 1S-2S transition. We determine the energy difference of 1S and 2S of Ps by detuning the laser frequency to search for the laser energy that makes the most 1S-2S transition. At the right frequency, the excess 2S detected by the MCP will be at the maximum.

Chapter 2

Theoretical background for 1S-2S excitation of Ps

The positronium (e^+e^-, Ps) and muonium (μ^+e^-, M) as the purely leptonic system are the ideal tools for testing the higher-order correction in Quantum Electrodynamics (QED), comparing to hadronic particles, like a hydrogen atom, that is subject to finite-size effects. The experiments on those bounded leptonic systems can be used to test CP violation and even Standard-Model-Extension.

The 1S-2S transition of positronium was first studied in 1982 [9]. The idea was shooting the positrons to a silica powder. The positrons will be captured by electrons and form positroniums. Then, the Ps will diffuse out of the silica powder. The Ps are then excited by a laser with a specific frequency to 2S state. Measuring such frequency (energy) of the laser w.r.t. the number of excited 2S Ps will form a line-profile.

2.1 Lorentzian line-profile

In the spectra of atom, spectral lines are always not strictly monotonic. The uncertainty principle states that the change in energy cannot be infinitely small given the time of observation is finite. Indeed, the spectra distribution $I(v)$ of the absorbance or emission frequency of atom form a Lorentzian shape around the center frequency $v_0 = (E_i - E_k)/h$, where E_i and E_k are the energy of two levels of transition.

The line shape corresponding to the spreads of E_i and E_k can be studied as a classic damped oscillator with frequency w, mass m, restoring force k and damping constant γ. By solving the differential equation

$$\ddot{x} + \gamma\dot{x} + \omega_0^2 x = 0, \tag{2.1}$$

one can obtain the approximate amplitude

$$x(t) \approx x_0 e^{-(\gamma/2)t} \cos(\omega_0 t) \tag{2.2}$$

with the assumption of small damping ($\gamma \ll \omega_0$) [10]. By applying the unilateral Fourier transform

$$A(\omega) = \frac{1}{\sqrt{2\pi}} \int_0^\infty x_0 e^{-(\gamma/2)t} \cos(\omega_0 t) e^{-i\omega t} \mathrm{d}t \tag{2.3}$$

which transforms the motion function to the frequency domain. The lower integration limit must be 0 because $x(t) = 0$ for $t < 0$. Thus, the equation above is solved as

$$A(\omega) = \frac{x_0}{\sqrt{8\pi}} \left(\frac{1}{i(\omega - \omega_0) + \gamma/2} + \frac{1}{i(\omega + \omega_0) + \gamma/2} \right). \tag{2.4}$$

Close to central frequency ω_0, where $(\omega - \omega_0)^2 \ll \omega_0^2$, one term is negligible and the intensity profile of the spectral line is obtained as

$$I(\omega - \omega_0) = \frac{C}{(\omega + \omega_0) + (\gamma/2)^2}, \tag{2.5}$$

where $C = I_0 \gamma / 2\pi$. The normalized Lorentzian profile is

$$L(\omega - \omega_0) = \frac{\gamma/2\pi}{(\omega + \omega_0) + (\gamma/2)^2}. \tag{2.6}$$

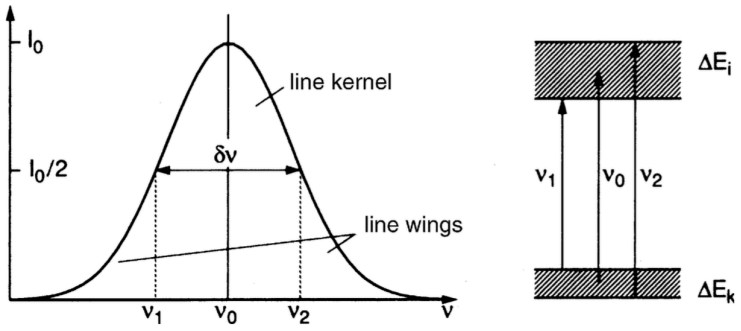

Figure 2.1: The line-profile of two-state transition. [10]

To note, the full halfwidth at half-maximum (FWHM) is defined as

$$\delta\omega_n = \gamma \quad \text{or} \quad \delta\nu_n = \gamma/2\pi = \Gamma/\pi. \tag{2.7}$$

2.2 Lifetime

The lifetime of exotic atom can be obtained by rearranging (2.1) to solve for the radiant power, which yields

$$\frac{\mathrm{d}W}{\mathrm{d}t} = P = -\gamma m x_0^2 \omega_0^2 e^{-\gamma t} \sin^2 \omega_0 t. \tag{2.8}$$

As the time average $\overline{\sin^2 \omega t} = 1/2$, the time-averaged radiant power is

$$\overline{\frac{\mathrm{d}W}{\mathrm{d}t}} = \overline{P} = -\frac{\gamma}{2} m x_0^2 \omega_0^2 e^{-\gamma t}, \tag{2.9}$$

which shows that the intensity I has the decay time of $\tau = 1/\gamma$. If taking into account of all the decay channels, Einstein coefficient A_i should be introduced to replace the damping coefficient γ as a more formal description of the frequency distribution of spontaneous emission corresponding to the line-shape. As stated in the uncertainty principle, $\Delta E_i \simeq \hbar/\tau_i$, the average lifetime τ_i of a specific transition energy ΔE_i is given by

$$\delta\omega = \Delta E_i/\hbar = 1/\tau_i. \tag{2.10}$$

In the case of our experiment,

$$\Delta E_i = \sqrt{\Delta E_{1S}^2 + \Delta E_{2S}^2}, \tag{2.11}$$

which means that the 1S-2S spontaneous transition depends on the energy uncertainties of these two levels.

Specifically, the lifetime of Ps depends on the specific Zeeman sublevels. For 1S, the ortho-Ps lifetime is 142 ns and the para-Ps is less than 1 ns. For 2S, the ortho-Ps lifetime is 1.1 μs and the para-Ps is 144 ns. In this experiment of exciting 1S to 2S, only very tiny fraction of 1S will be excited to 2S. The 2S Ps are mainly in the ortho-spin configuration, because Ps reach the MCP after excitation in 400 ns; most para-Ps should decay to photons before reaching MCP. The 1S Ps can only be in ortho-spin. Therefore, only 2S ortho-Ps annihilation should be detected as signal by MCP at the time window of 400 $\pm$ 50 ns.

Another prominent value to measure precisely is the lifetime of the ortho-Ps at 1S, which can be done with almost the same experiment set-up. With the precise measurement of 1S decay time and some corrections, its Hyperfine Structure (HFS) constants can be obtained. A rough illustration of this 1S decay phenomenon is shown in Fig. 6.2.

2.3 AC Stark effect

In this and the following section, the two-body Coulomb system is studied with the assumption that the driving laser is monochromatic and no three-photon transition happens. Due to the Selection Rule, 1S-2S transition cannot be single-photon, as its $|\Delta l| = 0$. There must be an intermediate level between 1S and 2S to make the transition possible [10]. So, the photon number must be greater than 1 but we only focus on the two-photon case now.

Consider the classic time-dependent Hamiltonian of a Ps that

$$H(t) = \hat{H}_0 + V(t), \tag{2.12}$$

where

$$\hat{H}_0 = \frac{\boldsymbol{P}^2}{m_e} - \frac{K_e e^2}{2r}, \tag{2.13}$$

$$\begin{aligned} V(t) &= V\frac{1}{2}[\exp(i\omega_L t) + \exp(-i\omega_L t)], \\ V &= -e\epsilon_L \hat{\boldsymbol{z}}. \end{aligned} \tag{2.14}$$

The potential $V(t)$ is an incident plane wave field. And, the dipole approximation is made for the interaction Hamiltonian.

We express the wavefunction of Ps as a superposition of the ground and excited states that

$$|\Psi(t)\rangle = c_g(t)\exp(-i\omega_g t)\,|g\rangle + c_e(t)\exp(-i\omega_e t)\,|e\rangle\,. \tag{2.15}$$

The solution to its Schrödinger equation is

$$\begin{aligned} \dot{c}_g &= i\frac{\Omega^*}{2}\exp(-i\Delta t)c_e(t), \\ \dot{c}_e &= i\frac{\Omega}{2}\exp(i\Delta t)c_g(t), \end{aligned} \tag{2.16}$$

where $|c_g|^2$ and $|c_e|^2$ represent the fraction of the population in the ground and excited state, respectively, and it obeys $|c_g|^2 + |c_e|^2 = 1$. Moreoever, we can define two new coefficients to replace them without changing physical meaning of the system.

$$\begin{aligned} c_g^{'}(t) &= c_g(t), \\ c_e^{'}(t) &= c_e(t)\exp(i\Delta t). \end{aligned} \tag{2.17}$$

The time derivative of these newly defined coefficients become

$$\begin{aligned} i\hbar\dot{c_g}^{'}(t) &= \frac{\hbar\Omega}{2}c_e^{'}(t), \\ i\hbar\dot{c_e}^{'}(t) &= \frac{\hbar\Omega}{2}c_g^{'}(t) - \hbar\Delta c_e^{'}(t). \end{aligned} \tag{2.18}$$

Apart from the formalism of coefficients above, the resonant Rabi frequency Ω for the system close to the resonance ($(\omega_l + \omega_a) \gg \Delta$) and frequency detuning Δ are defined as

$$\Omega = \frac{\langle e|\hat{\boldsymbol{z}}|g\rangle \cdot \vec{E}_0}{\hbar} = 2(2\pi\beta_{ge})I \qquad \Delta = \omega_l - \omega_a, \tag{2.19}$$

with the intensity of the plane wave

$$I = \frac{1}{2}\epsilon_0 c\mathcal{E}_L^2. \tag{2.20}$$

To match the density matrix formalism, we introduce the density operator ρ as

$$\rho = |\Psi\rangle\langle\Psi|, \tag{2.21}$$

so that ρ and c_i can be related through

$$\rho_{ge} = \langle g|\rho|e\rangle = \langle g|\Psi\rangle\langle\Psi|e\rangle = c_g c_e^*. \tag{2.22}$$

Following the definition in Eq.2.21 and Eq.2.22, the two level system the density matrix is simply

$$\rho = \begin{pmatrix} \rho_{ee} & \rho_{eg} \\ \rho_{ge} & \rho_{gg} \end{pmatrix}, \tag{2.23}$$

which has the correct physical meaning of the relative population in ground and excited state, as $\rho_{ee} + \rho_{gg} = 1$. ρ_{eg} and ρ_{ge} represent the coherences between those two states. This density matrix contains the information of Eq.2.15, while satisfying the our positronium bounded system condition showed in Eq.2.12

With the density matrix formalism set, we can now change our interest to the decay of 2S state of positronium. So, we describe the spontaneous emission as an exponential decay of the coherences at a constant rate, i.e.,

$$\left(\frac{\mathrm{d}\rho_{eg}}{\mathrm{d}t}\right)_{spon} = -\frac{\Gamma}{2}\rho_{eg}, \tag{2.24}$$

where Γ is the lifetime of the excited state. From here, we borrow from the Optical Bloch Equations to show

$$\begin{aligned} \dot{\rho}_{gg} &= \Gamma\rho_{ee} - \frac{i\Omega}{2}(\rho_{eg} - \rho ge) \\ \dot{\rho}_{ee} &= -\Gamma\rho_{ee} + \frac{i\Omega}{2}(\rho_{eg} - \rho_{ge}) \\ \dot{\rho}_{eg} &= (i\delta - \frac{\Gamma}{2})\rho_{eg} + \frac{i\Omega}{2}(\rho_{ee} - \rho_{gg}) \\ \dot{\rho}_{eg} &= (-i\delta - \frac{\Gamma}{2})\rho_{ge} - \frac{i\Omega}{2}(\rho_{ee} - \rho_{gg}). \end{aligned} \tag{2.25}$$

Then, we define the population difference to be $\omega = \rho_{gg} - \rho_{ee} = 1 - 2\rho_{ee}$, thus

$$\frac{\mathrm{d}\omega}{\mathrm{d}t} = \frac{\mathrm{d}\rho_{gg}}{\mathrm{d}t} - \frac{\mathrm{d}\rho_{ee}}{\mathrm{d}t} = \Gamma(1-\omega) - i\Omega(\rho_{eg} - \rho_{ge}); \tag{2.26}$$

consequently,

$$\dot{\rho}_{eg} = (i\delta - \frac{\Gamma}{2})\rho_{eg} + \frac{i\omega\Omega}{2}. \tag{2.27}$$

For the perturbation potential in steady-state, i.e., $\dot{\omega} = \dot{\rho}_{eg} = 0$, the conclusion is

$$\begin{aligned} \omega &= \frac{1}{1+s} \\ \rho_{eg} &= \frac{i\Omega}{2(\Gamma/2 - i\delta)(1+s)}, \end{aligned} \tag{2.28}$$

where $s = \frac{|\Omega|^2}{2|\Gamma/2-i\delta|^2} = \frac{\Omega^2/2}{\delta^2+\Gamma^2/4} = \frac{s_o}{1+(2\delta/\Gamma)^2}$ is the saturation parameter which indicates the degree of the system is saturated for the excited state [11]. So far, we have illustrated all the useful parameters and properties of the single-photon transition, and it is easy to get to the two-photon scenario.

For the case of our experiment, the two-photon transition matrix elements can be calculated by modifying the single-photon transition matrix elements. To obtain matrix elements, multiply Eq.2.23 with a known second-order perturbation $H^{(2)}$ [3]. For instance, one of the time-dependent two-photon transition matrix element is

$$\begin{aligned}\beta_{ge} &= \left\langle e\middle|V(t)\frac{1}{(E_g+\hbar\omega_L)-H_0}V(t)\middle|g\right\rangle \\ &= -\frac{e^2}{2hc\epsilon_0}\left\langle e\middle|z\frac{1}{H_0-(E_g+\omega_l)}z\middle|g\right\rangle,\end{aligned} \tag{2.29}$$

where E_g is just the energy of the ground state given by

$$E_g = -\frac{(Z\alpha)^2 m_e c^2}{2n^2}, \tag{2.30}$$

with α being the fine-structure constant. From Eq.2.15 the Hamiltonian of this two-level H can be obtained as

$$H = E_g|g\rangle\langle g| + E_e|e\rangle\langle e| + \frac{\hbar\Omega}{2}[\exp(i\omega_L t)+\exp(-i\omega_L t)]^2\cdot(|e\rangle\langle g|+|g\rangle\langle e|), \tag{2.31}$$

with the eigenvalue of each state defined as

$$\begin{aligned}E_g &= h\nu_g + h\Delta\nu_{ac}(g), \\ E_e &= h\nu_e + h\Delta\nu_{ac}(e).\end{aligned} \tag{2.32}$$

The frequency shift $\Delta\nu_{ac}$ is defined by

$$\Delta\nu_{ac} = \beta_{ac} I(t), \tag{2.33}$$

where β_{ac} is the AC Stark shift coefficient. The detailed calculation is described in [3] for hydrogen case. To calculate it specific for positronium it must be multiplied by a factor of

$$\frac{1}{Z^4}\left(\frac{m_e}{\mu}\right)^3 = 8, \tag{2.34}$$

where μ is the reduced mass for positronium which is $m_e/2$ and Z is the nuclear charge. Besides, I is the intensity of laser. For our set-up, the laser has the power of 1 kW and beam waist of 0.5 mm. So, the intensity is estimated as

$$I = \frac{P}{\pi w^2/2} \approx 2.55\times10^9 \text{ W/m}^2. \tag{2.35}$$

Combine Eq. 2.33 I calculate the AC Stark effect on the line-profile to be

$$\Delta\nu = 0.751 \text{ MHz (to the left)} \tag{2.36}$$

To compare, the natural linewidth of 1S-2S is approximately 1.26 MHz.

2.4 Doppler effect

In our experiment, the counter-propagating photon beam is used to excite the 1S positronium. The two-photon absorption can be described by a two-step process that goes from $|i\rangle$ through a virtual intermediate state $|v\rangle$ to the final state $|f\rangle$, thus by introducing a virtual state the probability amplitude from $|i\rangle \rightarrow |f\rangle$ is equivalent to the sum of probability amplitudes of $|i\rangle \rightarrow |v\rangle$ and $|k\rangle \rightarrow |f\rangle$ with detuning frequencies of $\omega - \omega_{ik}$ and $\omega - \omega_{kf}$ respectively.

We can modify the derived Lorentzian line-profile in Eq.2.6 to show the probability of transition as

$$\begin{aligned} A(\omega) = C\Delta N^0 I^2 \left| \sum_m \frac{(\boldsymbol{D}_{im}\hat{\boldsymbol{e}})(\boldsymbol{D}_{mf}\hat{\boldsymbol{e}})}{\omega - \omega_{im}} \right|^2 \\ \times \left(\exp\left[-\left(\frac{\omega_{if} - 2\omega}{2kv_p} \right)^2 \right] + \frac{kv_p}{\sqrt{\pi}} \frac{\gamma_{if}/2}{(\omega_{if} - 2\omega)^2 + (\gamma_{if}/2)^2} \right), \end{aligned} \tag{2.37}$$

where C is a normalization constant, ΔN^0 is the non-saturated population difference (can be derived using Eq.2.28), $\boldsymbol{D}$ is the matrix element of any transition and v_p is the most probable velocity of the positronium (we aim to measure time of fly (TOF) at the next stage). While ΔN^0 and $\boldsymbol{D}$ are completely from theory, once we have measured v_p, Eq.2.37 can be calculated numerically. Then, we can then expand this equation to quantify the effect of different orders of Doppler shift. The computational simulation is done with full details in [12].

To note, only second-order Doppler shift will be added to the systematic uncertainty for this experiment, while the first-order one does not count, because two counter-propagating photons set-up can eliminate its effect. The reason is also explained in [13]

Chapter 3

The cyclotron buffer gas trap

A cyclotron trap is used to store the positrons produced by the process that $Na^{22} \rightarrow Ne^{22} + \beta^+ + \nu_e$. This process has a branching ratio Γ/Γ_{tot} of 90.6% and the endpoint energy T_{max} of 545 keV. The lifetime of Na^{22} is 2.6 years, which is our radioactive source. Inside the trap, the average energy of the positrons is reduced to less than 7 eV by the buffer gas. A rotating magnetic field of certain frequency is used to constrain the motion of the positrons [14].

3.1 Principle of the cyclotron trap

The source provides a continuous moderated beam with the intensity of 20000 e^+s^{-1}. So, the energy must be extracted from the positrons to keep them trapped. A technique of rotating magnetic field is used to transfer the positron motion in the direction parallel to the field to perpendicular one. This technique is also called "virtual trapping", because some positrons will still be lost as their motions are not in correct phase with magnetic field rotating [15]. Thus, a buffer gas needs to be introduced to increase the trapping efficiency.

We arranged the pressure of the gas and the electric potential in a descendent order for five stages, so that the positrons will lose energy when passing the stages. Finally, the positrons will enter the last stage and eventually be trapped. A gate, at the exit of the last stage, with higher potential than all former stages is used to stop the positrons and scatter them back.

The energy distribution of the positrons still obeys the Boltzmann distribution, thus the energy spread is governed by the ambient temperature which is corresponding to the trapping gas. A cooling method could be used in the last stage to significantly decrease the energy spread of the positrons, which can simplify and improve the buncher (Cha.4).

3.2 Verification and optimization

We measured the energy distribution of the trapped positron by varying the gate voltage. In detail, we lowered the gate voltage for a short period of time (50 ns) and measure the number of positrons hitting the MCP. The result from the MCP w.r.t the gate voltage variation amplitude is plotted in Fig. 3.1. The voltage region (7.0 V to 8.0 V) of partial positrons passing through reveals the energy distribution of the trapped positrons.

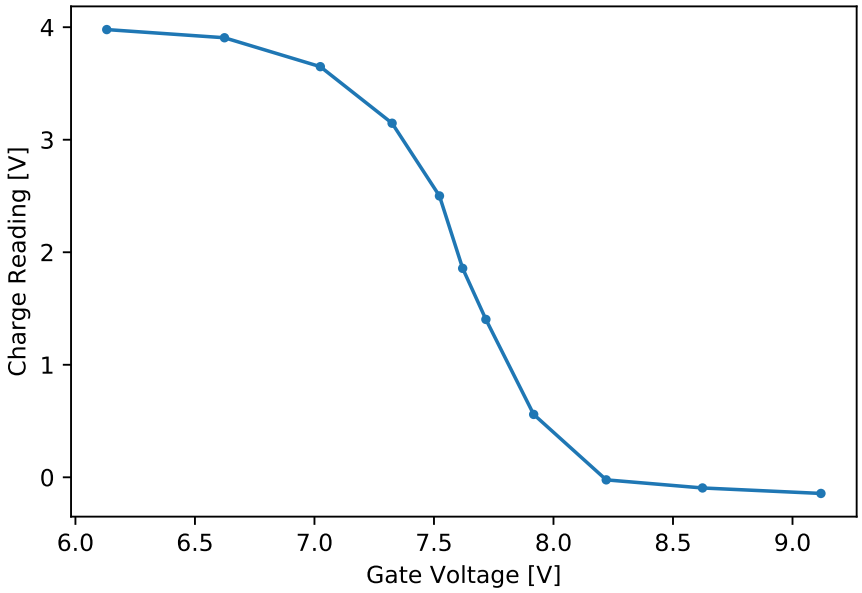

Figure 3.1: The measurement of the number of positrons pass through the gate w.r.t. the gate voltage

Therefore, differentiating Fig. 3.1 gives the positron number at any specific energy. This method of measuring is also used in [16]. Then, we fit a skewed gaussian function to the data, because the skewness is expected from the Bolzmann distribution. For fitting result, the mean μ and standard deviation σ are statistically meaningful for us.

The trap optimization is based on the fitting result of Fig. 3.2. The goal is to minimize σ while keeping other parameters float within a reasonable range. We wrote an automatic python script to control this experimental set-up to vary all the parameters one at a time and store the results. In the end, it generated a N-dimensional contour graph to show the local minimum points and their relevant parameters. The optimization parameters includes rotating magnetic field frequency, gas pressures, potentials and so on.

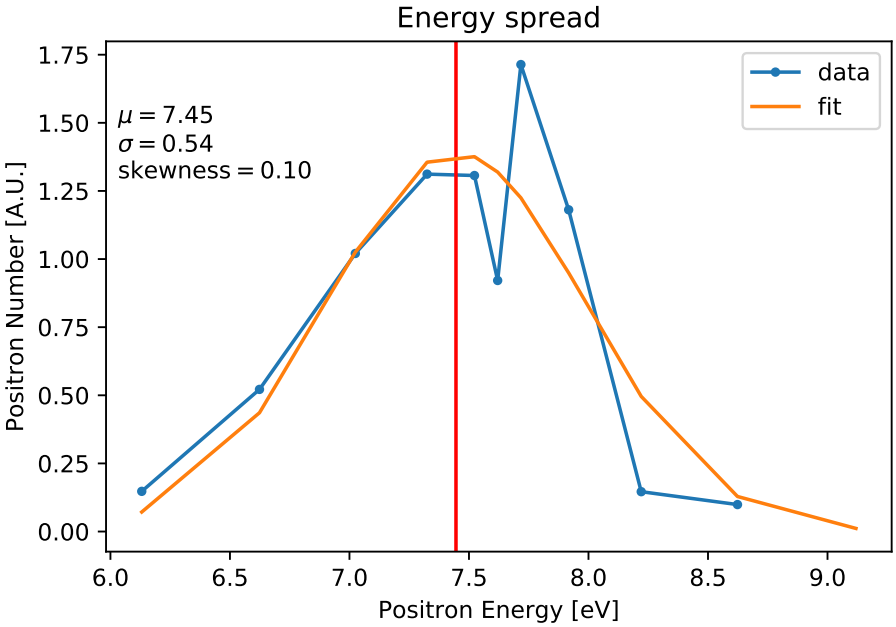

Figure 3.2: Differentiating of Fig. 3.1, the energy distribution of positrons is shown

The automatic script is a great way to alleviate human trial-and-error hard-work. Although the development of this script required lots of effort, the fitting result is surely the most optimized. At the time of this paper, σ was improved to be 0.54 from above 1.5 with the starting parameters, which were calculated from a theoretical simulation.

In the end, we interpolate the function in Fig. 3.1 and feed it into the MATLAB simulation, because the physical meaning of this function is the energy spread of the trapped positron. The function is shown in Fig. 4.2 as the input.

To conclude, in this section we first measured the energy distribution indirectly, then we introduced our Python script to automatically generate N-dimensional contour graph to optimize the energy spread of the trapped positrons. Finally, we used the measured distribution for input of the simulation of the buncher and it will be discussed in Cha. 4.2.

Chapter 4

Time compression of the positron beam

We implemented a short metal tube of less than 50 cm, as the buncher, to shorten the positron beam length. The buncher has the ability to fast varying its potential, by a pulse amplifier through a low capacitance cable.

The goal of this buncher is to change the energy of the positron according its position inside the beam, so that the beam will be compressed to less than 1 ns short when it reaches the target. To explain, after leaving the tube, the positrons will have gradient energy distribution with time such that latter ones will catch up earlier ones, so the arrival time at the target for all positrons will be the same.

4.1 Principle of the buncher

The buncher consists of a metal shield connected to an amplifier and a function generator. The voltage of the the buncher relative to the ground is given by the arbitrary waveform generator by the function generator and amplified by the amplifier. The energy of the positrons inside the buncher is assumed to be unchanged as they do not experience any electric force.

The bunching time was critically coupled to the gate to assure all positrons entered the buncher before the potential started to change. To assure that, we used some voltage offset, illustrated in Fig. 4.3, to reduce the speed of the positrons in the buncher.

A limiting factor to note is the rise-time of waveform, because current supply of the pulse amplifier is limited and capacitance of the circuitry is about ten to one hundred pf level. We must take this limited rise-time into account when forming our bunching waveform.

There is an analytical equation to generate the bunching waveform. It shows as

$$V_b(t) = V_0 + \frac{m_e l^2}{2q_e}(t_f - t)^{-2}, \tag{4.1}$$

where V_0 is the initial buncher potential relative to the ground, l represents the bunching length scale, and t_f is just a time offset [17].

This analytic solution is perfect for an ideal case, in which the positron beam is mono-energetic, and the ideal case is verified by the MATLAB simulation. However, for the real case, the energy spread is presented and will make the bunching ineffective. The energy spread of the initial beam is the most significant source of uncertainty in our experiment. I have presented a solution to it in Appendix A.

4.2 Simulation

We used an algorithm to convolute the energy and time distribution of the positron beam. In this way, we do not have to simulate each individual particle of its unique position and energy. Only matrix convolution is need in our algorithm to save computation time.

When the positrons passed a position in space, the energy coordinate will be added or subtracted weighted according to the buncher potential $V_b(t)$ and elevator potential $V_{el}(t)$. For example, varying the potential before the positrons started to leave the tube will not change their energy until they exit the tube; on the other hand, positrons leave at the same time will be added with the same energy. This implies that the energy spread will degrade the bunching effect.

From one frame to another, this algorithm simply added the time coordinate to get the next frame. Then, the convoluted matrix will give back the true distribution.

This algorithm is the perfect analog to the real physics scenario and can be studied for the case of non-ideal case if the real initial time-energy distribution is inputed.

The measurement of Fig. 3.2 was used as an input shown in Fig. 4.1. We also measured the real gate voltage waveform as another input to get this initial beam condition in Fig. 4.2. To note, we do not have a sharp edge on the beam, because the gate voltage was not a perfect square wave. Fortunately, this distortion from the gate will not affect our bunching.

In Fig. 4.3, it has an offset of 7 V to reduce the energy of the positrons. With the reduced speed, a slower bunching waveform can be used. Such offset was chosen for compensating the rise-time of the buncher.

In Fig. 4.4, we can see the energy of the positrons was reduced by the voltage offset to approximately 2 eV in the upper graph. The bottom graph demonstrate that the positrons were bunched and risen to the approximately energies of 65 eV. The positive slope is the sign of bunched.

After the buncher, we also applied a forward magnetic to constrain positron

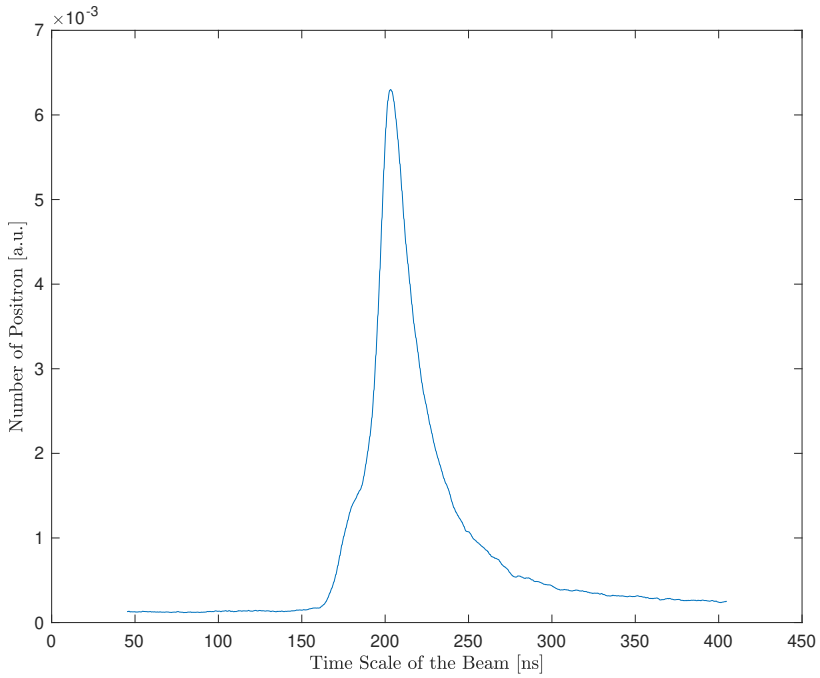

Figure 4.1: Measured time distribution of the beam

motion to prevent them hitting the tube. Then, the positrons reached the elevator, in which the potential was raised to 6 kV to assure their energy to be high enough for hitting the target.

In Fig. 4.5, the same logic was applied to the elevator to assure the positron beam did not have a high speed. In the upper graph, the average energy of the positrons was reduced to approximately 20 eV. In the lower graph, the energy was risen to above 6 KeV, because we want the beam to have very high energy when hitting the target. So, the positronums can be created. After the elevator, the positrons will hit the target in a very short time because of the high speeds.

At the target, we applied gaussian fit to the time distribution of the positrons. The σ of this shape in the Fig. 4.6 is 6.4, thus the FWHM of the arrival time is 16.6 ns. This result was not final because the bunching waveform had a large distortion.

To note, the waveform of the elevator can be improved by shorten the coaxis cable, which has the capacitance of 50 pf per meter. The rise time of 0 to 6 keV was more than 200 ns and was estimated to reduced to around 20 ns. With the fast rise-time, the elevator will be able to bunch the positrons even with 100 eV energy inside the elevator. Therefore, this will give us more voltage amplitude allowance to adjust the buncher waveform.

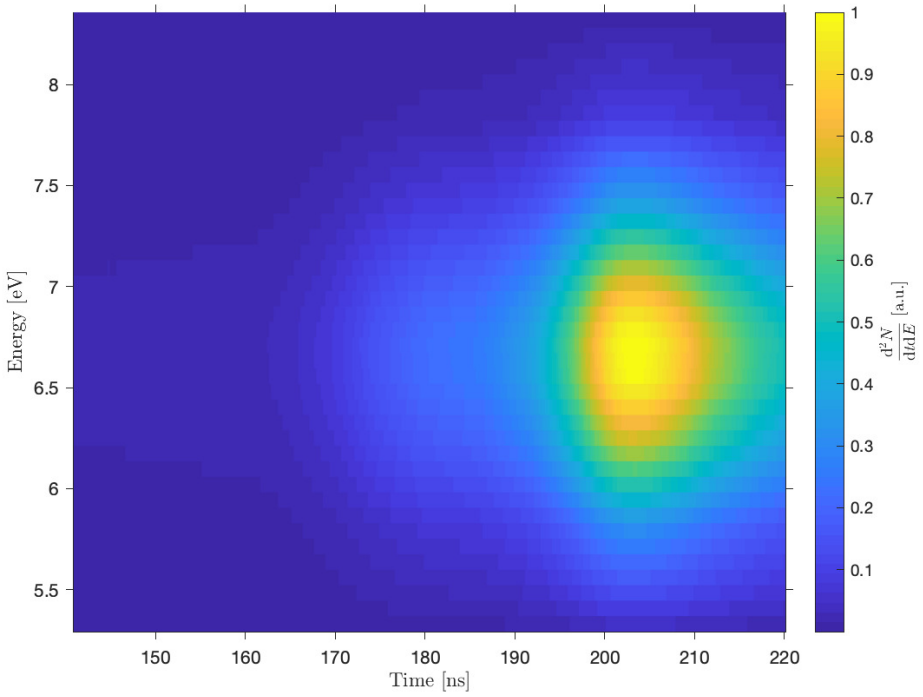

Figure 4.2: Real time and energy distribution inputed

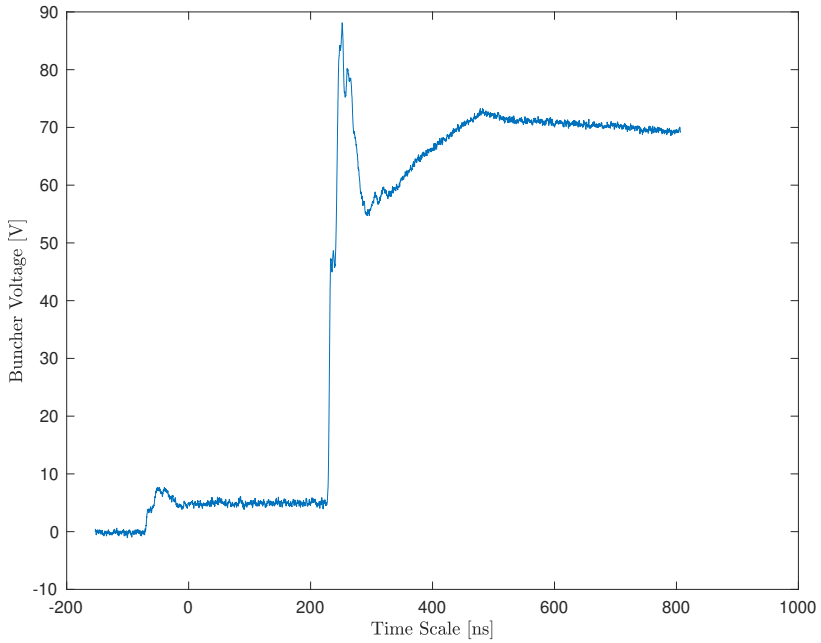

Figure 4.3: Measured real buncher waveform, generated according to the Eq. 4.1

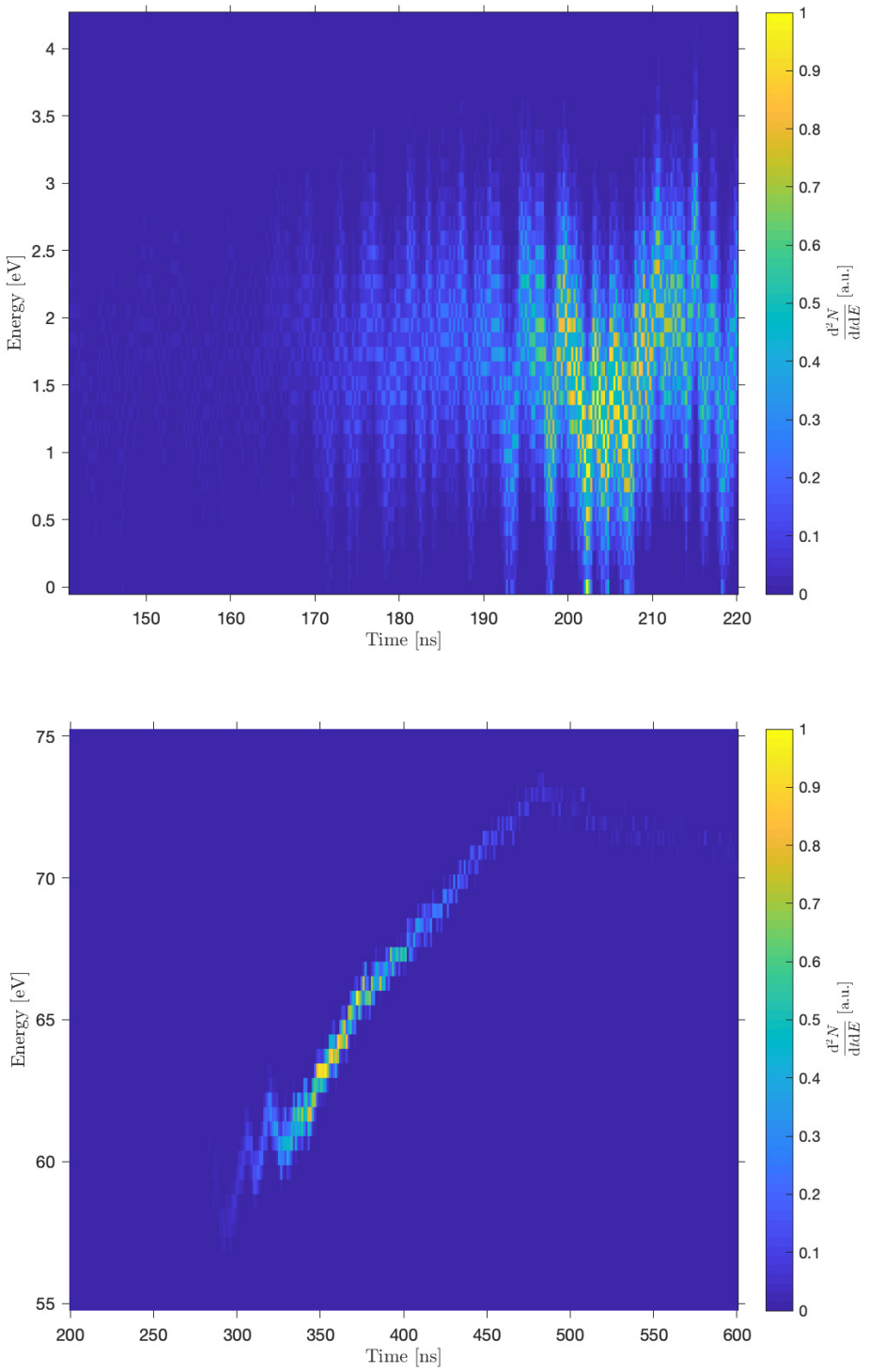

Figure 4.4: Simulated time and energy distribution at the entry of buncher (up) and at the exit of buncher (down)

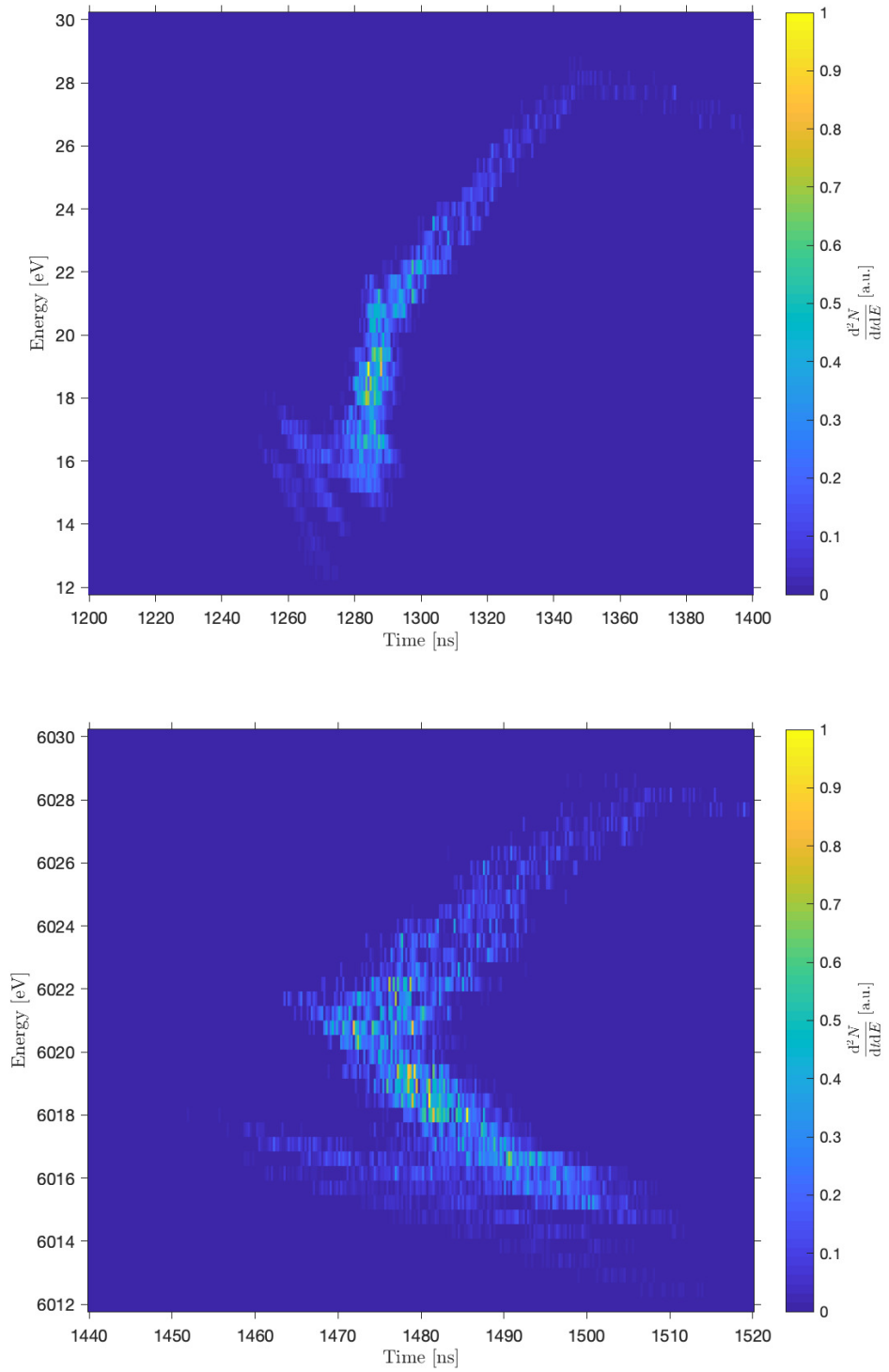

Figure 4.5: Simulated time and energy distribution at the entry of elevator (up) and at the exit of elevator (down).

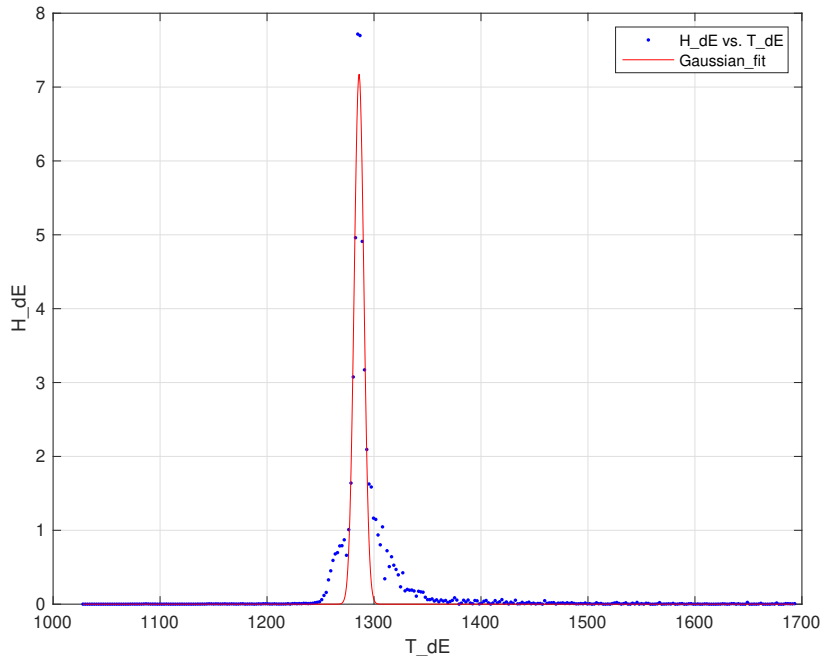

Figure 4.6: The number of positrons arrive at the target vs time

Chapter 5

Laser system

A fine-tuning laser centered at 486 nm wavelength is implemented for exciting the positrons to from 1S to 2S state. The laser system consists of a Toptica frequency stabilized CW laser, which corresponds to half the frequency of the transition. Since the CW laser alone cannot excite the 1S to 2S efficiently, an additional Radiant Dyes pulsed dye amplifier is used, which is pumped by a Spectra Physics pulsed Nd:YAG operating in the UV.

Given the natural linewidth is around 1.26 MHz, the laser can be detuned for a few hundreds of MHz to generate the line shape and find the central position. This system is able to deliver about 20 mJ energy for a single pulse of 7 ns.

5.1 Laser spectroscopy

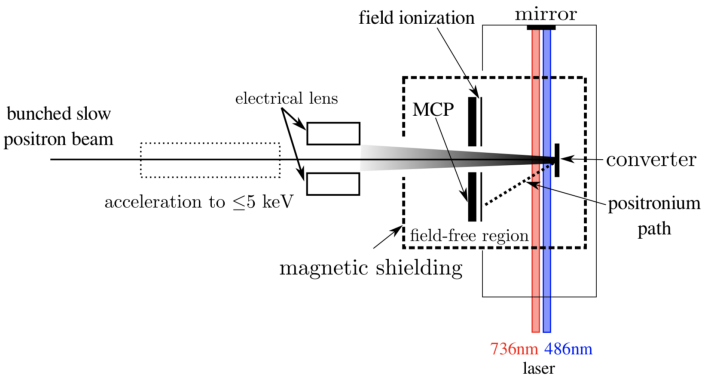

Figure 5.1: laser set-up for this experiment

As discussed in the theoretical background, the resonance line of an atom at rest can be described by a Lorentzian profile in (2.6). The full-width of half

maximum (FWHM) γ is known as the natural linewidth, which equals to $1/\tau$ the lifetime. In order to determine the center of the Lorentzian profile, a narrow peak is preferred. Therefore, a system with long lifetime is desirable. For our experiment, the 1S state of the Ps has life time of 142 ns and 2S has 1136 ns, corresponding to the natural linewidth of 1.26 MHz.

We used the technique called two-photon transition to eliminate the first-order Doppler effect. In the laser cavity, two counter-propagating photons will excite the Ps, which ensures that the frequency shift of two photons seen by the Ps is the same magnitude but of opposite signs. Therefore, the total excitation frequency is independence of the velocity of the Ps.

For this experiment set-up, the time-of-flight effect broadened the line-profile for approximately 40 MHz and the line-profile is also shifted by the second-order Doppler effect by around 60 MHz.

Chapter 6

Data analysis and results

We take the timed data flow from MCP, scintillator and two laser diodes. Each pulse of the positrons was counted as one event.

Since our MCP was only connect to a single cathode, there is no spatial resolution. The diodes are the indicators for the lasers' states. The blue laser on is the 2S signal flag. The red laser on is the 30S signal flag. Most importantly, the MCP data is used for searching potential signal.

In order to generate the line-profile of the 1S-2S transition, we detuned the blue laser to different frequencies. The 2S generated counts at that frequency should be proportional to the line-profile amplitude. At the specific laser frequency, at least 20,000 events were accumulated because the signal count probability was expected to be way less than 1 per event. If the background is well-suppressed, we are expected to observe a spike in the histogram.

6.1 Processing of raw data

For each release of the positrons, the MCP voltage reading is recorded in a time series as shown in Fig. 6.1. Then, we mark the spikes in the MCP data. This speaks are the possible decays of 2S.

There are two ways to detect peaks; one is to regard everything above certain threshold voltage as "signal", i.e., we can count more "signals" in wider peaks, while narrower peak has less "signals". This algorithm has problem with "big peak", which is from the 1S decay.

The improved algorithm was used to eliminate the multi-counting effect and increase the sensitivity of the "big peak" time interval. We detect local maximum of the MCP reading as peaks, thus width of the peaks has no effect on the number of "signal" we count. Besides, we can adjust the minimum time separation of the peaks to reject random noise. An example of a single event is shown in Fig. 6.1.

Next, we extract the events time and put them in the histogram for all events in the same TTree.

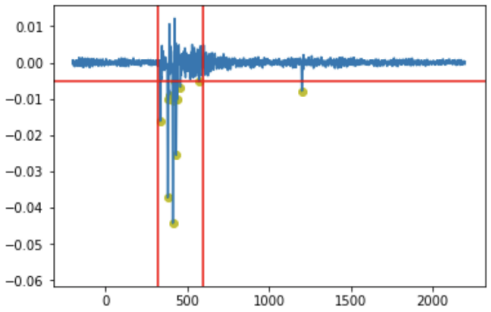

Figure 6.1: Peak detection example for a single time MCP reading voltage (V) vs time (ns). Horizontal red line is the threshold. Vertical red lines are the time interval of most scattered 1S detected. Dots indicates the detected peaks.

6.2 Improvement from implementation of the buncher

We have discussed the buncher in chapter 4, which compressed the beam length.

For the 1S decay, the scatter positrons should have a narrower peak in the histogram. In fact, we have detected such difference for old and new data. Although the MCP is tilted, the shape of the arrival does show a significant improvement, shown in Fig. 6.2. The fit of an exponential function is added to roughly show the decay time τ.

It is clear that the decay time of the graph of bunched beam is lesser in Tab. 6.1. Also, the systematic error for different measured data-set is checked to be not comparable larger than the given statistical error, and here it is ignored because these data-set are just too scarce and does not reflect true variance within group.

τ_{old} (s^{-1})	τ_{new} (s^{-1})
0.01254 ± 0.00034	0.00757 ± 0.00020

Table 6.1: The exponential fit value to two background shapes, standard deviation is given for statistical error.

6.3 Signal significance

The background-only data sets are collected under the condition that either the blue laser is off or the laser frequency is far off resonance. There should be no 2S excited in such data set.

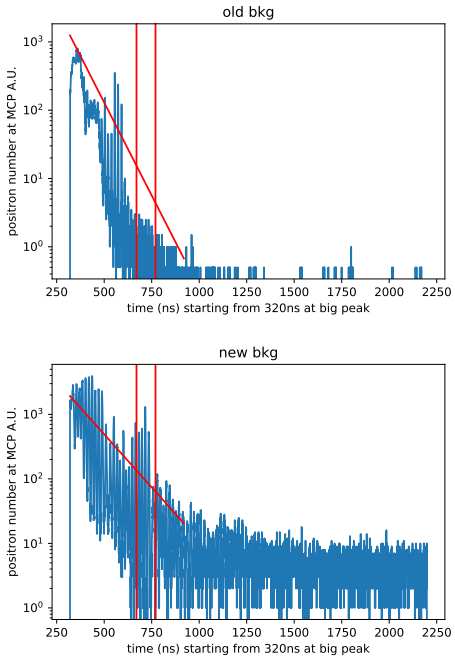

Figure 6.2: The MCP reading of w/o bunching and w/ bunching when laser is off. Vertical lines are for the time window of interest (expected 2S decay). A fit is also added.

One of the new background-only data set contains total of 3004 events, which includes 9924 peaks, roughly 3.3 peaks per event. We ran the same procedure to collect signal data set with blue laser on. Different frequencies were collected separately. Then, histogram of signal data sets were normalized to the number events w.r.t background-only. Four different frequencies are plotted. We integrated the histograms of prominent time interval.

The expect decay of 2S observed is 0.02-0.2 per event, resulting 60-600 events in that integrated interval. However, the signal counts are very close to 0. So, at this stage we have not observed an expected amount of 2S.

The results were plotted in Fig 6.3 with integrated signal events counts. The counts is the final result that shows the number of 2S by excitation at the given frequency.

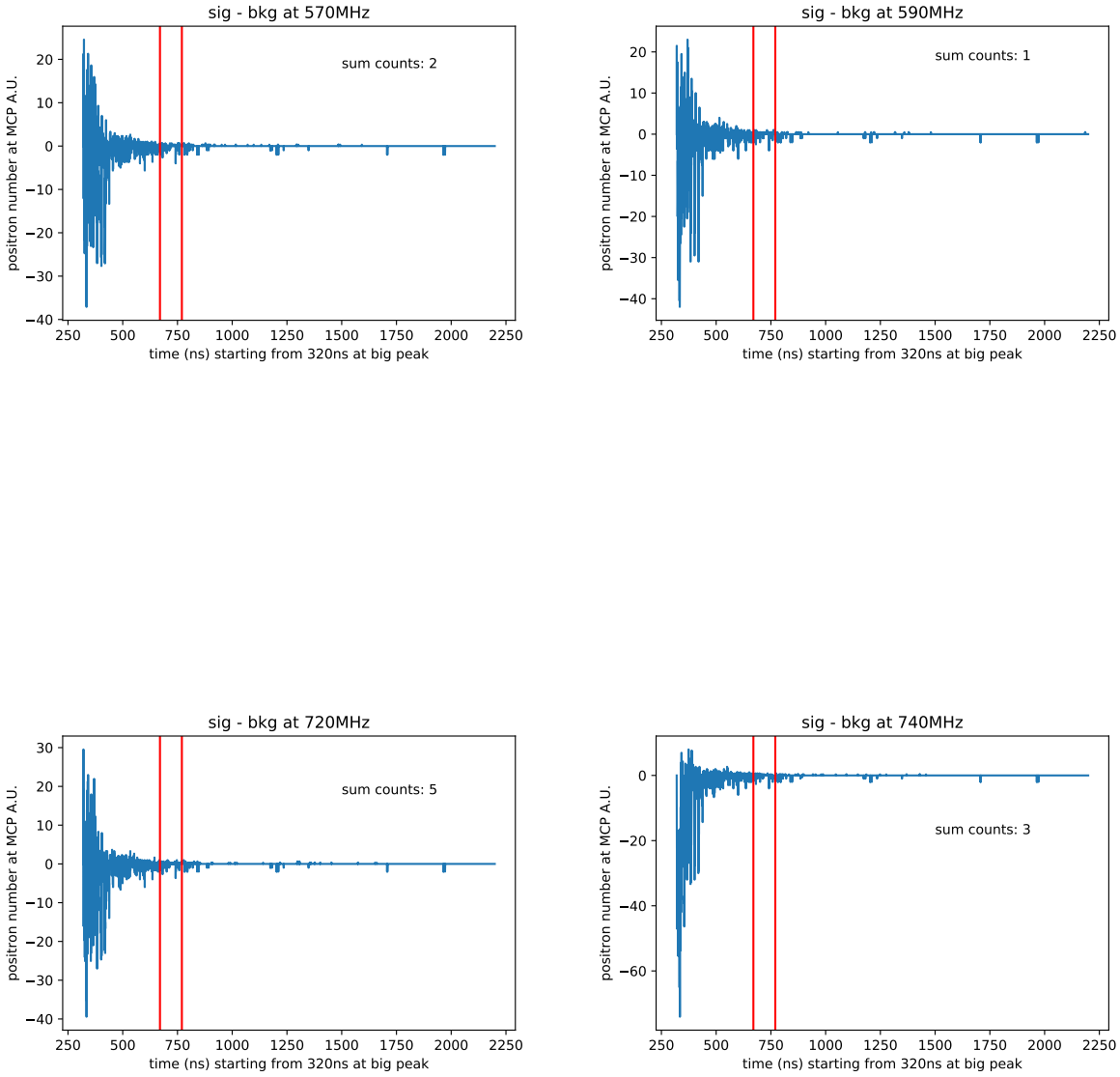

Figure 6.3: Histograms of signal happen time with red laser on (sig) minus that of red laser off (bkg). Red window is the probable signal period. The counts is the surplus of sig data set compare to bkg data set in red window.

Bibliography

[1] K. Pachucki and S. G. Karshenboim, Phys. Rev. A **60**, 2792 (1999).

[2] M. S. Fee et al., Phys. Rev. A **48**, 192 (1993).

[3] M. Haas et al., Phys. Rev. A **73**, 052501 (2006).

[4] M. W. Heiss, G. Wichmann, A. Rubbia, and P. Crivelli, Journal of Physics: Conference Series **1138**, 012007 (2018).

[5] M. Deutsch, Phys. Rev. **82**, 455 (1951).

[6] P. J. Mohr, B. N. Taylor, and D. B. Newell, Journal of Physical and Chemical Reference Data **41**, 043109 (2012).

[7] S. G. Karshenboim, Physics Reports **422**, 1 (2005).

[8] C. G. Parthey et al., Phys. Rev. Lett. **107**, 203001 (2011).

[9] S. Chu, A. P. Mills, and J. L. Hall, Phys. Rev. Lett. **52**, 1689 (1984).

[10] W. Demtröder, *Laser Spectroscopy: Vol. 1: Basic Principles*, Springer Science and Business Media, 4, illustrated edition, 2008.

[11] G. Grynberg, A. Aspect, and C. Fabre, *Introduction to quantum optics: from the semi-classical approach to quantized light*, Cambridge Univ. Press, New York, NY, 2010.

[12] Z. N. Burkley, High-power deep-uv laser for improved and novel experiments on hydrogen, PhD Dissertation, 2019.

[13] P. Crivelli, Physics of the simplest exotic atoms, submitted for the Habilitation as a Privat Dozent at ETH Zurich, 2019.

[14] L. Gerchow et al., Instruments **2** (2018).

[15] C. Surko, *Accumulation, storage and manipulation of large numbers of positrons in traps I — The basics*, pages 83–128, 2014.

[16] C. Vigo, Search for invisible decay channels of positronium confined in a vacuum cavity, 2017.

[17] D. A. Cooke et al., Journal of Physics B: Atomic, Molecular and Optical Physics **49**, 014001 (2015).

Appendix A

Outlook for buncher improvement

As we discussed earlier that the energy spread of the trapped positrons is the most significant source of error for the bunching.

We assume the energy distribution is invariant with time of extraction. The positrons will spread out as they travel some distance because their energy is different. We call this "sorting" effect, which is proportional to the distance of travel. If we have a long enough distance for the positron beam to "sort" before we bunch it, the energy and time distribution of the beam will have a negative slope and is illustrated in Fig. A.1.

Therefore, if we can simulate the "sorting" effect and use the lower graph as the input to generate bunching waveform. We will be able to eliminate the negative effect of large energy spread of the trapped positron. As a result, we can bunch the positron beam to be less than 1 ns.

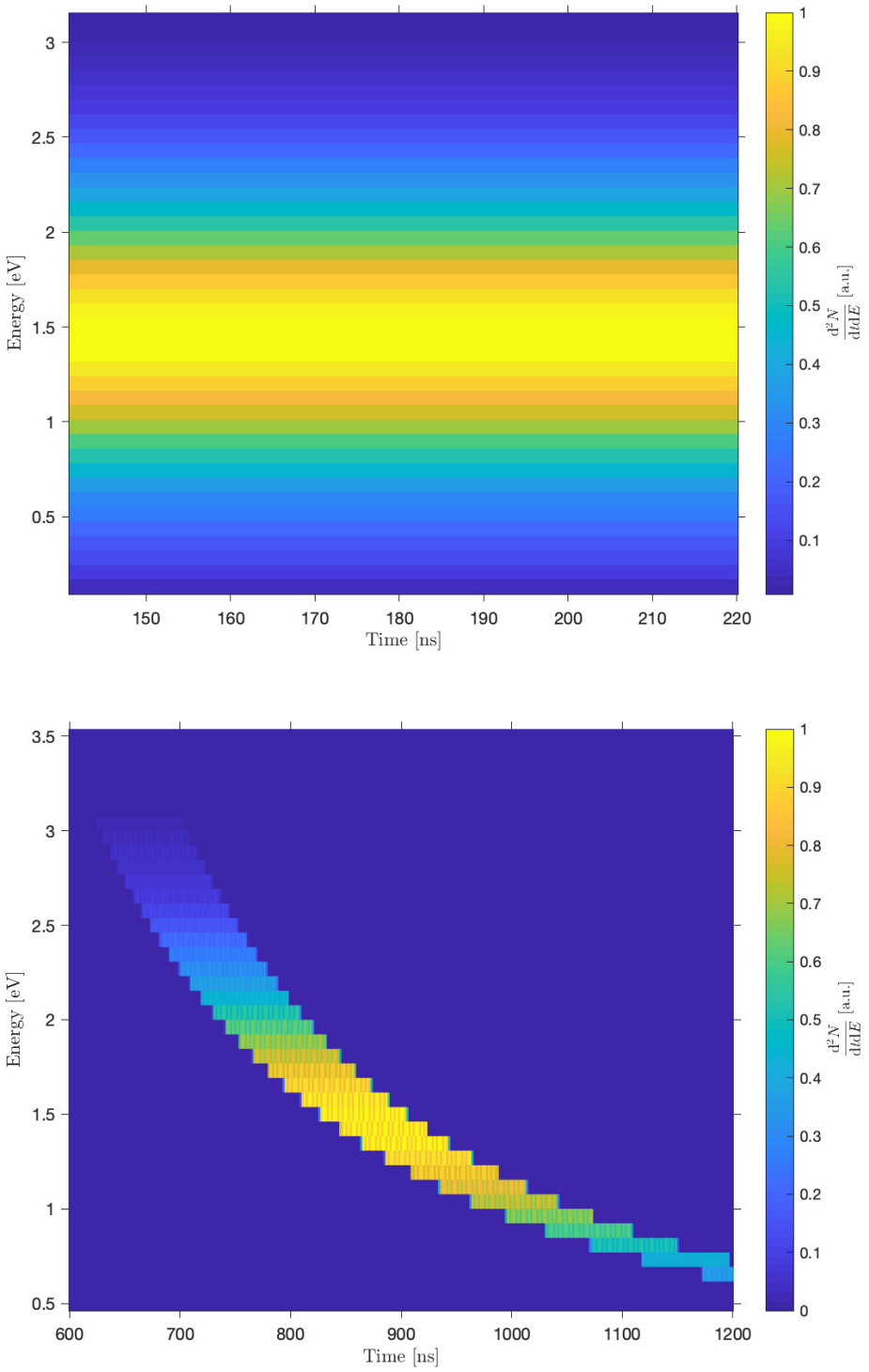

Figure A.1: Time spread out after 0.5 m of flying with real energy distribution but lower mean energy